Solution NMR structure of CsgE: Structural insights into a chaperone and regulator protein important for functional amyloid formation

Qin Shu[a], Andrzej M. Krezel[a], Zachary T. Cusumano[b], Jerome S. Pinkner[b], Roger Klein[b], Scott J. Hultgren[b], and Carl Frieden[a,1]

[a]Department of Biochemistry and Molecular Biophysics, Washington University School of Medicine, St. Louis, MO 63110; and [b]Department of Molecular Microbiology, Washington University School of Medicine, St. Louis, MO 63110

Contributed by Carl Frieden, May 11, 2016 (sent for review March 28, 2016; reviewed by James G. Bann and Thomas J. Silhavy)

Curli, consisting primarily of major structural subunit CsgA, are functional amyloids produced on the surface of *Escherichia coli*, as well as many other enteric bacteria, and are involved in cell colonization and biofilm formation. CsgE is a periplasmic accessory protein that plays a crucial role in curli biogenesis. CsgE binds to both CsgA and the nonameric pore protein CsgG. The CsgG–CsgE complex is the curli secretion channel and is essential for the formation of the curli fibril in vivo. To better understand the role of CsgE in curli formation, we have determined the solution NMR structure of a double mutant of CsgE (W48A/F79A) that appears to be similar to the wild-type (WT) protein in overall structure and function but does not form mixed oligomers at NMR concentrations similar to the WT. The well-converged structure of this mutant has a core scaffold composed of a layer of two α-helices and a layer of three-stranded antiparallel β-sheet with flexible N and C termini. The structure of CsgE fits well into the cryoelectron microscopy density map of the CsgG–CsgE complex. We highlight a striking feature of the electrostatic potential surface in CsgE structure and present an assembly model of the CsgG–CsgE complex. We suggest a structural mechanism of the interaction between CsgE and CsgA. Understanding curli formation can provide the information necessary to develop treatments and therapeutic agents for biofilm-related infections and may benefit the prevention and treatment of amyloid diseases. CsgE could establish a paradigm for the regulation of amyloidogenesis because of its unique role in curli formation.

biofilm formation | intrinsically disordered protein | aggregation | protein–protein interaction | CsgG

CsgE is a nonsecreted periplasmic accessory protein essential for curli biogenesis (1, 2). *Escherichia coli, Salmonella* spp., and many other *Enterobacteriaceae* produce functional amyloid fibers, called curli, on their surfaces (3–6) that are involved in cell adherence, invasion, host colonization, and biofilm formation (6–11). Curli fibers make up the primary proteinaceous component of the extracellular matrix in pellicle biofilm, a subset of biofilms formed by the cystitis uropathogenic *E. coli* isolate UTI89 (12). The formation of biofilms represents a common strategy by which bacteria resist mechanical and chemical clearance mechanisms of the host (13–15). Biofilms can facilitate the persistence and recurrence of infections (16, 17), lead to the colonization of medical devices with resistant organisms (18, 19), and increase transmission of foodborne illnesses (20). It is therefore important to understand the mechanism of curli biogenesis to develop treatments and therapeutic agents in biofilm-related infections (21).

The formation of the curli, however, is a surprisingly complex process being produced via the extracellular nucleation-precipitation pathway or the type VIII secretion system (22). Seven products (CsgA, CsgB, CsgC, CsgD, CsgE, CsgF, and CsgG) of two operons (*csgBAC* and *csgDEFG*) cooperate to facilitate curli fiber formation (2, 23, 24). Curli fibers are primarily composed of the major structural subunit, CsgA (2–4), but also contain a small amount of the minor structural subunit, CsgB (25, 26). Although CsgA is prone to aggregation and forms amyloid fibers in vitro (2, 27), the formation of curli fibers in vivo is nucleated by CsgB (28–30). CsgC exists in periplasm and is an effective inhibitor of CsgA polymerization, suppressing fibrilization at substoichiometric ratios as low as 1:500 (CsgC:CsgA) (31), and perhaps preventing premature periplasmic amyloid formation and toxicity to the bacterium.

The genes encoding the biosynthetic machinery responsible for curli fiber assembly are located on *csgDEFG*. This separate, divergently transcribed operon is found upstream of *csgBAC* and begins with the gene known to encode the master curli transcriptional regular, CsgD (23, 32). CsgD controls expression of the *csgBAC* operon as well as the biosynthesis of cellulose, the primary polysaccharide component of the biofilm extracellular matrix (33–35). CsgE and CsgF are also encoded by the operon and have long been considered accessory proteins that function in concert with CsgG, the outer membrane pore responsible for the translocation of CsgA and CsgB to the outer membrane space (1, 2, 36–38). CsgG forms a symmetric, nonameric, ungated, and nonselective protein secretion channel, as revealed recently (37, 39). CsgF is secreted to the cell surface, binds to CsgG, and appears to be critical for the specific localization of CsgB (38).

Numerous studies have provided insights into the role of CsgE in curli biogenesis. Deletion of *csgE* results in decreased stability and secretion of CsgA, CsgB, and CsgF in vivo (1, 36, 38). CsgE inhibits CsgA fibrillation at a ratio of 1:1 in vitro (1) and also

Significance

Curli are functional amyloids produced on the surface of many gram-negative bacteria. These amyloids, consisting primarily of CsgA, are involved in cell adhesion, colonization, and biofilm formation. CsgE is a periplasmic accessory protein that plays a central role in curli biogenesis by its interaction with CsgA and with the pore protein CsgG. To understand the mechanism of curli formation, it is critical to determine the structure of the proteins that are required for their formation. Here, we report the atomic solution structure of a double mutant of CsgE, as determined by NMR. The study reveals unique structural features of CsgE and provides insights into the assembly of the secretion channel and the regulation of curli biogenesis.

Author contributions: Q.S., S.J.H., and C.F. designed research; Q.S., A.M.K., Z.T.C., and J.S.P. performed research; Q.S., A.M.K., Z.T.C., R.K., S.J.H., and C.F. analyzed data; and Q.S., R.K., S.J.H., and C.F. wrote the paper.

Reviewers: J.G.B., Wichita State University; and T.J.S., Princeton University.

The authors declare no conflict of interest.

Data deposition: The atomic coordinates have been deposited in the Protein Data Bank, www.pdb.org (PDB ID code 2NA4). The NMR chemical shifts have been deposited in the BioMagResBank, www.bmrb.wisc.edu (accession no. 25927).

[1]To whom correspondence should be addressed. Email: frieden@biochem.wustl.edu.

This article contains supporting information online at www.pnas.org/lookup/suppl/doi:10.1073/pnas.1607222113/-/DCSupplemental.

prevents the curli-dependent pellicle biofilm formation by *E. coli* at the air–liquid interface of a static culture (40). Recently, cryo-EM data have shown that CsgE binds to the periplasmic domain of CsgG with 9:9 (CsgE:CsgG subunit) stoichiometry and forms a capping adaptor that closes off the periplasmic face of the CsgG secretion channel (37). The CsgG–CsgE complex has a preconstriction chamber (~24,000 Å^3), probably entrapping substrates such as CsgA and facilitating the entropy-driven diffusion across the outer membrane (37). Hence, CsgE appears to interact with CsgA as a periplasmic chaperone that delivers the structural subunits to the periplasmic vestibule of the CsgG pore. The CsgE and CsgG interaction is vital for efficient and specific curli transport through the pore.

Despite the established role these subunits play in curli assembly, the transport details of curli subunits, especially the major subunit CsgA, have yet to be fully elucidated. Until now, the lack of a high-resolution CsgE structure has hindered our ability to understand how CsgE interacts with CsgA, CsgG, and itself to direct curli transport. One primary barrier to structure elucidation has been the mixture of oligomeric species formed by purified CsgE. However, we have recently used molecular footprinting techniques to generate a double mutant of CsgE (W48A/F79A) that is more stable and monodispersed at high concentrations (41). As shown here, the behavior of this double-mutant CsgE appears to be similar to that of the WT protein in overall structure and function. Moreover, the double mutant does not oligomerize at concentrations required for structure determination by NMR. Here, we report an NMR structure of the mutated CsgE. Our results suggest the mechanism of CsgE in the assembly of curli secretion channel and will be critical for understanding the interaction of CsgE with other proteins involved in curli formation.

Results

Comparison of Structure and Activity of WT CsgE and Mutant CsgE W48A/F79A. Wild-type (WT) CsgE tends to self-associate to oligomers in a concentration- and temperature-dependent manner. In our previous report, residues responsible for the oligomerization have been identified by hydrogen-deuterium amide exchange coupled with mass spectrometry, and a double-mutant CsgE W48A/F79A was found to undergo significantly less self-association and to be more stable than the WT protein (41). As illustrated in Fig. 1, purified WT CsgE at 50 μM and 4 °C appears to be mostly monomeric but contains a small amount of nonameric oligomer. Both the main monomer peak (red *) and the minor nonamer peak (red arrow) are greatly retarded on size-exclusion chromatography (SEC) (Fig. 1 and Fig. S1). The double mutant, in contrast, eluted as a single peak (blue *) with a good approximation of monomeric molecular weight on SEC (Fig. 1 and Fig. S1). Native spray mass spectrometry of the peaks shown in Fig. 1 confirms that the observed peaks represent WT CsgE and the mutant protein (Fig. S2). When visualized using native-PAGE, WT CsgE migrates as a smear, whereas the double-mutant W48A/F79A migrates as a single band (inset of Fig. 1). The unusual retention of WT CsgE on SEC column and native-PAGE gel is probably a result of the interaction between the charged residues around W48 and F79 and the residual charges of SEC resin or gel matrix (discussed later). It may also relate to the dynamic equilibrium of monomers and nonamers of WT CsgE. The equilibrium between these species in vivo has been suggested to have functional consequences (24).

As noted earlier, NMR studies of WT CsgE are hindered as a result of the oligomerization of the protein at concentrations required for NMR. The self-association of WT CsgE can be partially prevented in the presence of low concentrations of urea, guanidine (Gdn), or arginine (Arg) (Fig. S3), but the resultant NMR spectrum is not sufficient for determining a structure at atomic resolution. However, these spectra are useful for inferring the overall structure, as most peaks are resolved and widespread in the 2D ^{1}H-^{15}N heteronuclear single quantum correlation (HSQC) spectrum, indicating that the protomer of WT CsgE is well-structured.

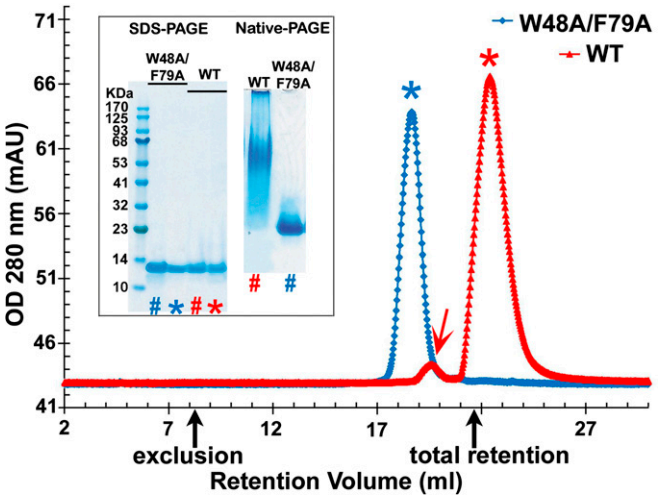

Fig. 1. Overlay of the representative SEC of purified WT CsgE (red trace) and W48A/F79A double mutant (blue trace). Black arrows mark the void and total retention volume of the column, determined using standard markers. The retention volume of the double-mutant W48A/F79A corresponds to a SEC-molecular weight about 13 kDa, according to the standard globular molecules (Fig. S1), consistent with the native spray mass spectrometry measurement (Fig. S2). However, purified WT CsgE partitioned into two distinct peaks (marked with red arrow and *), although it showed a single band on SDS/PAGE (*Inset*). The retention volume of the main peak (~90%, red*) is greater than the total retention volume. The measured mass of this main peak (red*) by native spray mass spectrometry (Fig. S2) is about 13,212 Da, confirming it is the monomeric WT molecule. The oligomeric peak of WT (red arrow) could not be measured by our native spray mass spectrometry. The approximate ratio of the SEC molecular weight for the main (red*) and minor (red arrow) peaks was about 1:9 (Fig. S1), suggesting the minor peak (red arrow) of WT on SEC is a nonamer, consistent with the previous report (37). On SDS- and native-PAGE (*Inset*), lane # was the same sample as loaded in SEC analysis; lane * was the peak marked * in SEC for WT CsgE and W48A/F79A CsgE.

The double mutant of CsgE shows well-resolved NMR spectra with little or no self-association at concentrations required for NMR (Figs. S4 and S5). More important, the double mutant is similar to WT in activity and overall structure. For example, Fig. 2*A* and Fig. S6 show that the double mutant is able to complement curli fiber formation to the same extent as WT when expressed on a plasmid in *ΔcsgE* MC4100 *E. coli* cells. Further, Fig. 2*B* demonstrates that the double mutant has the same inhibitory effect on CsgA aggregation as WT CsgE in vitro. Additional studies confirm that the secondary and tertiary structures of CsgE are not significantly altered in the double mutant. Fig. 2*C* shows that the CD spectra of WT and the double mutant are identical. In the 2D ^{1}H-^{15}N HSQC spectra (Fig. 2*D*), the distribution of most cross peaks of WT is similar to that of the double mutant, even though the peak intensities and line-shapes of WT are not as uniform as in the double mutant. The small subset of peaks that are shifted represents residues adjacent to the mutation sites (labeled in red, Fig. 2*D*) or located at the flexible and susceptible regions of the structure (labeled in green, Fig. 2*D*). Collectively, these findings indicate that the double mutant is a good representative of WT CsgE.

Structure of W48A/F79A CsgE. The calculations of NMR structures of W48A/F79A CsgE converge well, as indicated in the ensemble of 20 structures (Fig. 3*A*) and the low rmsd (Table S1).The core of the structure comprises a layer of two α-helices (α1 and α2) and a layer of three-stranded antiparallel β-sheet (β1–β3) (Fig. 3*B*). Both the N termini (A1–A5) and C termini (S99–F108) are highly flexible (Fig. 3*B*).

The closest structural neighbor for CsgE, as found by the VAST (Vector Alignment Search Tool) search service (42), is the N-terminal domain of TolB (PDB: 2W8B_A) (43), the β-propeller

BIOCHEMISTRY

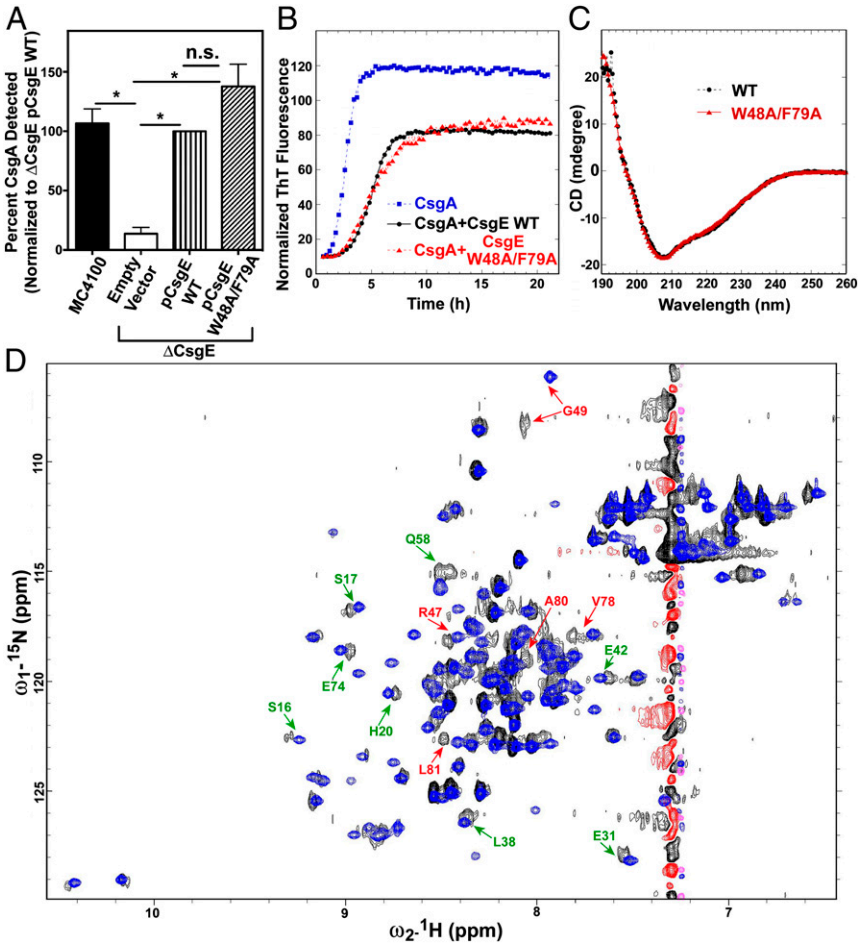

Fig. 2. Comparison of WT CsgE and the CsgE double mutant. (*A*) Quantification of curli production was determined by Western blot analysis of CsgA, as described in the *Materials and Methods*. (*B*) ThT assay of CsgA (4 μM) in the presence or absence of WT CsgE (1 μM) or the double-mutant W48A/F79A (1 μM). (*C*) Far UV-CD spectra. Both WT and the mutant protein were 10 μM in 20 mM potassium phosphate at pH 7.4, at 25 °C. (*D*) 2D ^{1}H-^{15}N HSQC spectra. Both WT and the mutant protein were 100 μM in 0.5 M arginine, 20 mM potassium phosphate at pH 5.8, and 10% (vol/vol) D_2O at 25 °C.

protein of Gram-negative bacteria Tol system (Fig. S7). Interestingly, CsgG is also structurally homologous with TolB, as reported previously (37). The topology of W48A/F79A CsgE is partially similar to CsgG and its homologs (Fig. S7). We conclude that the structural fold of CsgE belongs to the class of alpha and beta proteins (a+b) (Structural Classification of Proteins database), and that the structure of CsgE is a rudimentary form of the CsgG or the anticodon-binding domain-like fold.

A striking feature gleaned from the CsgE structure is the distribution of the surface electrostatic potential. There is a remarkable polar distribution of positive and negative residues along the surface of CsgE. The approximately goldfish-shaped (oval-shaped) molecular surface has positively charged residues clustered at the head end and negatively charged residues at the tail end, whereas the central region presents a neutral surface (Fig. 4). The positively charged "head" comprises basic residues located at the β1β2 hairpin loop (R43 and R47) and the β3α2 loop (K70 and R71). The negatively charged "tail" is formed by acidic residues located at the flexible N and C termini and the α1β1 loop. It is likely that the regions with concentrated charges mediate interactions with the main curli structural subunit CsgA and the membrane pore protein CsgG. This possibility is supported by the assembly model of the CsgG–CsgE complex discussed here.

Discussion

Assembly Model of the Curli Secretion Channel. The binding of CsgE to the nonameric CsgG pore results in the capping of the periplasmic vestibule (37). To probe the assembly mechanism of the curli secretion channel, we examined a 3D reconstruction of the CsgG–CsgE complex and the cryo-EM density, using the NMR structure of the CsgE double mutant and the crystal structure of CsgG. It is clear that nine copies of CsgE with nonameric CsgG are required to fit well into the cryo-EM density map of the CsgG–CsgE complex [Electron Microscopy Data Bank (EMD) ID: 2750] (Fig. 5), confirming the nonameric symmetry of CsgE in binding to CsgG and forming the channel complex. However, the precise assembly model cannot be clearly identified at the current resolution of the cryo-EM density map (~24 Å for EMD

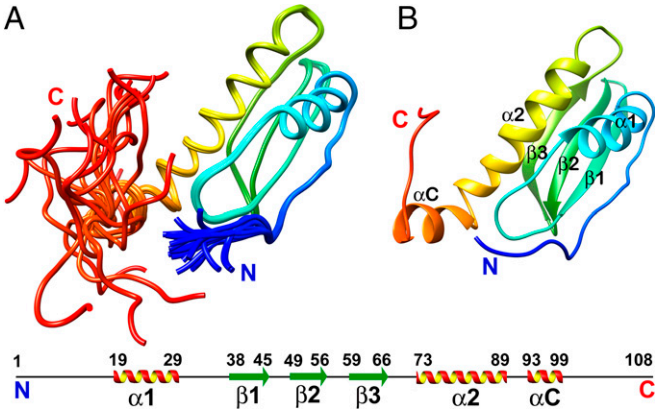

Fig. 3. Representative structure of W48A/F79A rainbow colored as blue to red from the N to C termini. (*A*) Ensemble of 20 structures. (*B*) Secondary structure elements are labeled according to the anticodon-binding domain-like fold, with the additional N and C terminal. The 6xHis-tag at the C terminal of the protein is not shown in the structure.

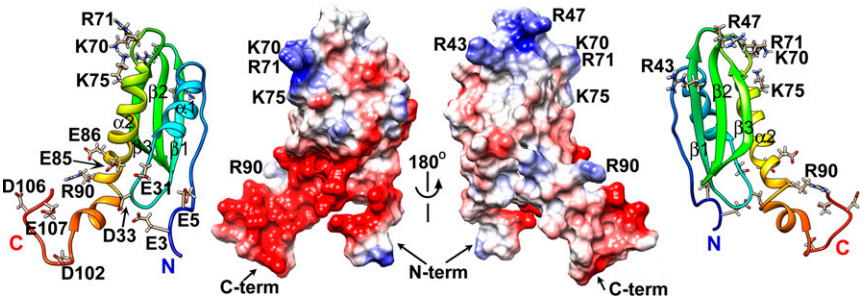

Fig. 4. Electrostatic potential surface of the CsgE double mutant. The surface residues that are positively (blue) or negatively (red) charged are also shown on the corresponding ribbon diagrams.

ID 2750). Thus, the individual residues responsible for CsgE self-association and CsgE/CsgG interactions cannot be easily identified. Furthermore, the orientation of the oval-shaped CsgE can be either a head-center model (illustrated in Fig. 5) or a tail-center model. CsgE nonamers are able to fit into the EM density in both opposite orientations. We prefer the head-center model based on the surface charge distribution. The main reason is that the surfaces of CsgG in the periplasmic vestibule are dominated by positive charges (residues R93, K94, R97, and R110 located around the α2 helix of CsgG), as shown in Fig. 5*C* (periplasmic view and slab view) and Fig. S8. The surface of CsgE has a remarkable polar distribution of charged residues, as described earlier, and the flexible tail side of CsgE is negatively charged (Fig. 4 and Fig. 5*B*). In the head-center model, the flexible and negatively charged tail of CsgE interacts with the periplasmic interface of the CsgG nonamer dominated by positive charges, driven by the electrostatic interaction between CsgE and CsgG.

The basic residues located at the head of CsgE, around R47 and K70, form a remarkable positively charged ring at the center of the nonameric CsgE cap (Fig. 5*B*). The eyelet of the CsgE nonamer is formed by the loop β1β2, where R47 is located. CsgA is the major substrate secreted through the CsgG–CsgE channel during curli biogenesis. Interestingly, the predicted structure of CsgA assembled within the fiber (44) has negatively charged surfaces resulting from exposed aspartate and glutamate residues (Fig. S9). Therefore, CsgA, even in disordered form, may use electrostatic interactions to specifically bind to the positively charged head of a monomeric CsgE or the center of the CsgE nonamer. The combined functions of a chaperone and the cap (or gate) of the secretion channel allow CsgE to stabilize unfolded sections of CsgA competent for transport by preventing CsgA from assuming more compact or entangled states. However, the temporal order of the CsgE nonamerization event and CsgE–CsgA interactions are unknown.

The current head-center model (Fig. 5) needs further refinement. First, the single-channel current recordings of phospholipid bilayer-reconstituted CsgG showed a total loss in CsgG conductivity, that is, a full blockage of the channel, upon CsgE binding (37). Therefore, the CsgE protomers need to be adjusted to pack tightly in the apex of the CsgE nonamer to close the channel but not clash with other regions. Second, analysis of the bile salt sensitivity of *E. coli* SLR12 and the mutations around the α2 helix of CsgG have shown that N88, L90, N91, and I95, located at the deeper part of the CsgG periplasmic mouth, interfere with CsgE, but R97, at a more accessible position, does not (37). The formation of the CsgG–CsgE complex probably involves hydrophobic interactions, and some part of CsgE has to access the deeper part of the CsgG periplasmic mouth. Both mechanisms require the dynamic conformation changes on CsgE and CsgG binding (further discussed later). Using the current static picture (Fig. 5), it is impossible to show the dynamic conformation changes on CsgE binding to CsgG. Our NMR data show that the tail side of CsgE protomer is highly flexible. Thus, we propose that the formation of the CsgG–CsgE complex is a dynamic process with multiple steps. The electro-negative and flexible tail of CsgE can adjust toward the electro-positive patches on the CsgG interface as the initial step in binding, and then some part of CsgE access into the CsgG periplasmic mouth deeper, and the flexible N and C termini of CsgE can stabilize in a rigid conformation fitting into the cryo-EM density completely. After the electrostatics-driven binding and some conformational change, there is also some hydrophobic packing between CsgE and CsgG, which strengthens and regulates the curli secretion channel.

Oligomerization of CsgE. As noted earlier, WT CsgE oligomerizes to different molecular weight forms, especially nonamers. WT CsgE has an unusual elution profile, and both monomeric and nonameric peaks are retarded on SEC. The NMR structure of CsgE provides insights into the unique properties of the molecule. Although the precise residues responsible for the self-assembly of CsgE oligomers have not been explicitly identified, the structure of the double-mutant CsgE suggests that hydrophobic

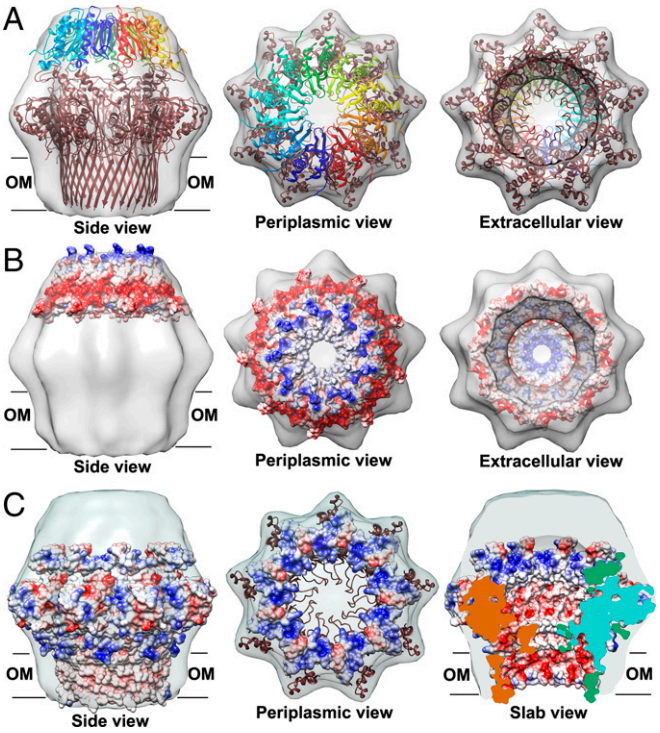

Fig. 5. Cryo-EM density (EMD ID: 2750) fitting of the CsgG–CsgE complex with the crystal structure of CsgG nonamer (4UV3) and nine copies of the solution NMR structure of double-mutant CsgE W48A/F79A (2NA4). (*A*) Both CsgE (colored as a blue to red rainbow by models) and CsgG (colored brown) were fitted in the cryo-EM density. Electrostatic potential surfaces of a nonamer of (*B*) CsgE and (*C*) CsgG. The surfaces of CsgG in periplasmic view are shown only 20 Å of depth to highlight the interface with CsgE in *C*. The flexible tail side of CsgE is negatively charged (Fig. 5*B* and Fig. 4). In contrast, the surfaces of CsgG at the periplasmic vestibule are dominated by positive charges (Fig. 5*C* and Fig. S8).

BIOCHEMISTRY

interactions promote the self-oligomerization of the protein. In the CsgE structure, the surface of the main body is mostly uncharged, and the majority of its hydrophobic residues are buried. However, as shown in Fig. S10, there are three clusters of hydrophobic and aromatic residues that are solvent exposed in the CsgE structure: cluster 1, V15 and Y23; cluster 2, W48, W51, F65, F67, and L69; and cluster 3, V78, F79, and I82. Cluster 2, especially, shows a highly exposed hydrophobic region. The clustered distribution of exposed hydrophobic residues in CsgE structure agrees with our previous study, using hydrogen–deuterium amide exchange coupled to mass spectrometry (41), showing regions 23–36, 39–51, and 67–79 are involved in CsgE self-association. The structural position of the exposed hydrophobic residues suggests the double mutant W48A/F79A can disrupt the main exposed hydrophobic cluster, resulting in weaker propensity to self-associate. Thus, we propose that the hydrophobic clusters around W48 and F79 are related to the self-oligomerization of CsgE.

The disruption of the hydrophobic clusters appears to not only change the oligomerization of CsgE but also locate conformation and flexibility of charged residues nearby. WT CsgE, both monomeric and nonameric forms, has an unusual retarded SEC profile, but W48A/F79A does not (*Results*). In the NMR structure, the positive charged residues located at the head side of CsgE, such as R47, which is near W48, are partially restricted in conformation because of the hydrophobic clusters nearby (cf. Fig. 4 and Fig. S10). It is possible that partially restricted positive charges bind/stick to the residual charges (mostly $-SO_3^-$) of the SEC resin and result in the retarding of WT CsgE. Mutations disrupting the exposed hydrophobic clusters may increase locate flexibility of those charged residues, and thus decrease the binding between CsgE and the residual charges in SEC resin.

Although it exists as a nonameric complex in vivo, preoligomerization seems not to be required for CsgE binding to CsgG. The oligomerization or, more specifically, nonamerization of CsgE seems not to be essential for the interaction of CsgE with either CsgG or CsgA. The structural mechanism of our proposed electrostatic interaction between CsgE and CsgA or CsgG is either via the positively charged head of CsgE binding to CsgA or the flexible negatively charged tail to CsgG (discussed earlier). Both interfaces are distant from the hydrophobic clusters of CsgE, which are the possible self-association sites. Although the data suggest that CsgE can associate with CsgG (or CsgA) regardless of its oligomeric state, additional experiments will be required to fully understand the influence of WT CsgE oligomerization in curli biogenesis.

Role of Dynamics in the Function of CsgE. The NMR structure presented here indicates that both the C and N termini of double-mutant CsgE are flexible. This disorder could functionally relate to the interaction of CsgE with CsgG, as discussed earlier in the assembly model. The helical region α2 and the disordered regions surrounding α2 in CsgG (illustrated in Fig. S8) have been suggested to be important in binding the components involved in the formation of curli fibers (37). The flexible tail side of CsgE can complex and permitting CsgA transport. Some structural disorder and dynamics of both CsgE and adapt to the binding surfaces of CsgG nonamer, promoting the assembly of the CsgG–CsgE CsgG permit the conformational adjustment upon the assembly, opening, and closing of the channel.

CsgE and the Intrinsically Disordered Protein CsgA. CsgE appears to interact with the intrinsically disordered CsgA through electrostatic interactions, which is probably important both for preventing the mislocalized or premature CsgA polymerization and for regulating the curli biosynthetic pathway in vivo. Some protein amyloids are linked to diseases, such as Alzheimer's disease, Parkinson's disease, diabetes type 2, and the spongiform encephalopathies (mad cow disease) (45). Many proteins can form amyloid-like fibrils in vitro, but they are not always detrimental or linked to disease in vivo. The relationship between amyloid formation in vitro and amyloid diseases in vivo is not clear. Interestingly, functional amyloids have been identified in bacteria, fungi, insects, invertebrates, and humans, including a constituent of bacterial curli, fungi hydrophobins, and human Pmel17 in melanosomes (2, 46, 47). Functional amyloidogenesis in these systems requires tight regulation of the protein–protein interactions to avoid toxicity in the cell. Intrinsic chaperoning or regulatory factors can control protein aggregation in these different protein systems, thereby preventing unwanted aggregation and enabling the biological use of functional amyloids. Knowledge of the chaperones and regulators involved in functional amyloid systems such as CsgE may provide unique clues to the prevention and treatment of amyloid diseases.

Conclusion

In addition to their established role in microbial colonization and biofilm formation, curli can serve as a model for studying the regulated production of functional amyloids. In this study, we report the structural properties of WT CsgE and the solution NMR structure of a mutant W48A/F79A. The results provide structural insights into the assembly of the curli secretion channel and regulation of curli secretion and biogenesis.

Materials and Methods

Reagents, strain and plasmid construction, protein preparation, and so on are presented in *SI Materials and Methods*.

SEC. The purified proteins were concentrated to 50 μM and loaded (200 μL) into a Superdex 200 10/300 (GE Healthcare) column at 4 °C. The elution buffer for SEC was 50 mM potassium phosphate, 150 mM NaCl at pH 7.4, running at 0.4 mL/min.

Measurement of Curli Production in Vivo. As previously described (1, 2, 38), curli production was induced by growth on CR-YESCA agar for 48 h at 26 °C. Qualitative measurement of curli production was monitored by visualization of Congo red binding. To quantify curli production, bacteria were scraped from YESCA plates, resuspended in 1 mL PBS, and normalized to an OD_{600} of 1.0. After normalization, a 200-μL volume of the cell suspension was pelleted and resuspended in 200 μL hexafluoro-2-propanol (HFIP) and incubated at room temperature for 10 min. After the 10-min incubation, HFIP was removed by vacuum centrifugation and the remaining pellet resuspended in 100 μL of 1× SDS-loading buffer and boiled at 100 °C for 5 min. Ten microliters of each sample was run on a 15% (wt/vol) SDS/PAGE gel and transferred overnight onto a PVDF membrane at a constant voltage of 40 V. Membranes were blocked in a solution of 5% (wt/vol) milk and 0.1% Tween-20 in PBS. Detection of CsgA was performed with a polyclonal antibody, as previously described (1), with immune blots developed by chemiluminescence (Super SignalWest Femto; Thermo Fisher). Images were captured using a CCD camera-based system (ChemiDoc; BioRad). Protein level analysis of CsgA was quantitated by densitometry of captured images, using Quantity One analysis software (version 4.6.9, BioRad).

Effect of WT or Double-Mutant CsgE on the Fibrilization of CsgA Monitored by Thioflavin T Fluorescence. Fibrilization of CsgA was followed by the fluorescence change of thioflavin T (ThT), as described elsewhere (27, 29). The activity difference between WT CsgE and the double mutant in vitro was analyzed by ThT assay. The kinetic measurements were carried out on a PTI spectrofluorometer (Photon Technology International, Inc.), using an excitation wavelength of 438 nm and emission wavelength of 490 nm, with continuous stirring at 25 °C. The protein concentration was 4 μM for CsgA in the absence or presence of 1 μM CsgE WT or W48A/F79A in 50 mM potassium phosphate, 150 mM NaCl, 25 μM ThT at pH 7.4, in a total volume of 1 mL.

Circular Dichroism. Far-UV CD spectra were recorded on a Jasco-J715 spectropolarimeter, using a 0.1-cm path length cuvette with temperature controlled at 25 °C. The protein concentration was 10 μM in 20 mM potassium phosphate at pH 7.4.

NMR Spectroscopy. NMR spectra were collected on Bruker AVANCE III 600, UltraStabilized800, and DMX 750 MHz spectrometers equipped with cryogenic triple-resonance probes. The proton chemical shifts were internally referenced to 2, 2-dimethyl-2-silapentane-5-sulfonic acid. The chemical shifts of ^{13}C and ^{15}N were referenced indirectly to 2, 2-dimethyl-2-silapentane-5-sulfonic acid, using the absolute frequency ratios. All NMR data were processed using Bruker TopSpin 3.2 and analyzed using the program NMRFAM-SPARKY (48).

Chemical Shift Assignment. The standard set of triple-resonance experiments was used for the backbone and side chain resonance assignments of CsgE W48A/F79A; spectra including 2D ^{1}H-^{15}N HSQC, ^{1}H-^{13}C HSQC (aromatic), ^{1}H-^{13}C HSQC (aliphatic), and 3D HNCO, HNCA, HNCOCA, CBCANH, CBCA(CO)NH, C(CO)NH, H(CCO)NH, aromatic (H)CCH-COSY, and aromatic ^{13}C-resolved NOESY. The 6xHis-tag at the C terminus of the protein was excluded from assignment and structure determination because of the deficiency of NMR signal probably caused by its flexible conformation and high solvent exchange rates. The assignments are illustrated in 2D ^{1}H-^{15}N HSQC (Fig. S3). The completeness is more than 96% without the C-terminal 6xHis-tag. The chemical shifts have been deposited in the Biological Magnetic Resonance Data Bank under accession number 25927.

Structure Calculation. Distance restraints based on nuclear Overhauser effect (NOE) were obtained from ^{1}H-^{15}N-NOESY-HSQC, ^{1}H- ^{13}C-NOESY-HSQC (aliphatic carbons), and ^{1}H-^{13}C-NOESY-HSQC (aromatic carbons) experiments in H_2O with mixing times of 100 ms. Peak picking and NOE assignment were performed using NMRFAM-SPARKY and in combination with CYANA (49). Distance restrains were obtained using the automated NOE assignment and structure calculation protocol available in CYANA (49, 50). Torsion angle restraints were calculated using TALOS-N (51), based on backbone H, N, Cα, Cβ, and CO chemical shifts. The initial 990 structures were calculated in CYANA, using the distance and torsion angle restrains. The 100 structures with the lowest target functions from CYANA were refined in AMBER 12 (ambermd.org), using only distance restrains. The refined structures were validated with the Protein Structure Validation Software suite 1.5 (psvs-1_5-dev.nesg.org) and PROSESS (www.prosess.ca). The 20 conformers with the lowest distance violations and best Z-scores were chosen and deposited in the Protein Data Bank under accession ID 2NA4. The structural statistics are shown in Table S1. All figures of structures were prepared with UCSF Chimera (1.10.2).

ACKNOWLEDGMENTS. We thank Ms. Hanliu Wang (Center for Biomedical and Bioorganic Mass Spectrometry, Department of Chemistry) for mass spectrometry analysis and Dr. Karen Dobson (Department of Molecular Microbiology, School of Medicine, Washington University) for the helpful discussions and review of this manuscript. This work is supported by NIH Grant R01 AI099099 (to S.J H. and C.F.).

1. Nenninger AA, et al. (2011) CsgE is a curli secretion specificity factor that prevents amyloid fibre aggregation. *Mol Microbiol* 81(2):486–499.
2. Chapman MR, et al. (2002) Role of Escherichia coli curli operons in directing amyloid fiber formation. *Science* 295(5556):851–855.
3. Olsén A, Jonsson A, Normark S (1989) Fibronectin binding mediated by a novel class of surface organelles on Escherichia coli. *Nature* 338(6217):652–655.
4. Collinson SK, Emödy L, Müller KH, Trust TJ, Kay WW (1991) Purification and characterization of thin, aggregative fimbriae from Salmonella enteritidis. *J Bacteriol* 173(15):4773–4781.
5. Collinson SK, Emödy L, Trust TJ, Kay WW (1992) Thin aggregative fimbriae from diarrheagenic Escherichia coli. *J Bacteriol* 174(13):4490–4495.
6. Barnhart MM, Chapman MR (2006) Curli biogenesis and function. *Annu Rev Microbiol* 60:131–147.
7. Kikuchi T, Mizunoe Y, Takade A, Naito S, Yoshida S (2005) Curli fibers are required for development of biofilm architecture in Escherichia coli K-12 and enhance bacterial adherence to human uroepithelial cells. *Microbiol Immunol* 49(9):875–884.
8. Vidal O, et al. (1998) Isolation of an Escherichia coli K-12 mutant strain able to form biofilms on inert surfaces: Involvement of a new ompR allele that increases curli expression. *J Bacteriol* 180(9):2442–2449.
9. Austin JW, Sanders G, Kay WW, Collinson SK (1998) Thin aggregative fimbriae enhance Salmonella enteritidis biofilm formation. *FEMS Microbiol Lett* 162(2):295–301.
10. Saldaña Z, et al. (2009) Synergistic role of curli and cellulose in cell adherence and biofilm formation of attaching and effacing Escherichia coli and identification of Fis as a negative regulator of curli. *Environ Microbiol* 11(4):992–1006.
11. Blanco LP, Evans ML, Smith DR, Badtke MP, Chapman MR (2012) Diversity, biogenesis and function of microbial amyloids. *Trends Microbiol* 20(2):66–73.
12. Hung C, et al. (2013) Escherichia coli biofilms have an organized and complex extracellular matrix structure. *MBio* 4(5):e00645–13.
13. Hall-Stoodley L, Costerton JW, Stoodley P (2004) Bacterial biofilms: From the natural environment to infectious diseases. *Nat Rev Microbiol* 2(2):95–108.
14. Fux CA, Costerton JW, Stewart PS, Stoodley P (2005) Survival strategies of infectious biofilms. *Trends Microbiol* 13(1):34–40.
15. Solomon EB, Niemira BA, Sapers GM, Annous BA (2005) Biofilm formation, cellulose production, and curli biosynthesis by Salmonella originating from produce, animal, and clinical sources. *J Food Prot* 68(5):906–912.
16. Costerton JW, Stewart PS, Greenberg EP (1999) Bacterial biofilms: A common cause of persistent infections. *Science* 284(5418):1318–1322.
17. Hatt JK, Rather PN (2008) Role of bacterial biofilms in urinary tract infections. *Curr Top Microbiol Immunol* 322:163–192.
18. Habash M, Reid G (1999) Microbial biofilms: Their development and significance for medical device-related infections. *J Clin Pharmacol* 39(9):887–898.
19. Costerton JW, Montanaro L, Arciola CR (2005) Biofilm in implant infections: Its production and regulation. *Int J Artif Organs* 28(11):1062–1068.
20. Kim SH, Wei CI (2009) Molecular characterization of biofilm formation and attachment of Salmonella enterica serovar typhimurium DT104 on food contact surfaces. *J Food Prot* 72(9):1841–1847.
21. Cegelski L, et al. (2009) Small-molecule inhibitors target Escherichia coli amyloid biogenesis and biofilm formation. *Nat Chem Biol* 5(12):913–919.
22. Desvaux M, Hébraud M, Talon R, Henderson IR (2009) Secretion and subcellular localizations of bacterial proteins: A semantic awareness issue. *Trends Microbiol* 17(4):139–145.
23. Hammar M, Arnqvist A, Bian Z, Olsén A, Normark S (1995) Expression of two csg operons is required for production of fibronectin- and congo red-binding curli polymers in Escherichia coli K-12. *Mol Microbiol* 18(4):661–670.
24. Van Gerven N, Klein RD, Hultgren SJ, Remaut H (2015) Bacterial amyloid formation: Structural insights into curli biogensis. *Trends Microbiol* 23(11):693–706.
25. Hammar M, Bian Z, Normark S (1996) Nucleator-dependent intercellular assembly of adhesive curli organelles in Escherichia coli. *Proc Natl Acad Sci USA* 93(13):6562–6566.
26. Bian Z, Normark S (1997) Nucleator function of CsgB for the assembly of adhesive surface organelles in Escherichia coli. *EMBO J* 16(19):5827–5836.
27. Wang X, Smith DR, Jones JW, Chapman MR (2007) In vitro polymerization of a functional Escherichia coli amyloid protein. *J Biol Chem* 282(6):3713–3719.
28. Hammer ND, Schmidt JC, Chapman MR (2007) The curli nucleator protein, CsgB, contains an amyloidogenic domain that directs CsgA polymerization. *Proc Natl Acad Sci USA* 104(30):12494–12499.
29. Shu Q, et al. (2012) The E. coli CsgB nucleator of curli assembles to β-sheet oligomers that alter the CsgA fibrillization mechanism. *Proc Natl Acad Sci USA* 109(17):6502–6507.
30. Hammer ND, et al. (2012) The C-terminal repeating units of CsgB direct bacterial functional amyloid nucleation. *J Mol Biol* 422(3):376–389.
31. Evans ML, et al. (2015) The bacterial curli system possesses a potent and selective inhibitor of amyloid formation. *Mol Cell* 57(3):445–455.
32. Zakikhany K, Harrington CR, Nimtz M, Hinton JC, Römling U (2010) Unphosphorylated CsgD controls biofilm formation in Salmonella enterica serovar Typhimurium. *Mol Microbiol* 77(3):771–786.
33. Prigent-Combaret C, et al. (2001) Complex regulatory network controls initial adhesion and biofilm formation in Escherichia coli via regulation of the csgD gene. *J Bacteriol* 183(24):7213–7223.
34. Brombacher E, Dorel C, Zehnder AJ, Landini P (2003) The curli biosynthesis regulator CsgD co-ordinates the expression of both positive and negative determinants for biofilm formation in Escherichia coli. *Microbiology* 149(Pt 10):2847–2857.
35. Brombacher E, Baratto A, Dorel C, Landini P (2006) Gene expression regulation by the Curli activator CsgD protein: Modulation of cellulose biosynthesis and control of negative determinants for microbial adhesion. *J Bacteriol* 188(6):2027–2037.
36. Robinson LS, Ashman EM, Hultgren SJ, Chapman MR (2006) Secretion of curli fibre subunits is mediated by the outer membrane-localized CsgG protein. *Mol Microbiol* 59(3):870–881.
37. Goyal P, et al. (2014) Structural and mechanistic insights into the bacterial amyloid secretion channel CsgG. *Nature* 516(7530):250–253.
38. Nenninger AA, Robinson LS, Hultgren SJ (2009) Localized and efficient curli nucleation requires the chaperone-like amyloid assembly protein CsgF. *Proc Natl Acad Sci USA* 106(3):900–905.
39. Cao B, et al. (2014) Structure of the nonameric bacterial amyloid secretion channel. *Proc Natl Acad Sci USA* 111(50):E5439–E5444.
40. Andersson EK, et al. (2013) Modulation of curli assembly and pellicle biofilm formation by chemical and protein chaperones. *Chem Biol* 20(10):1245–1254.
41. Wang H, Shu Q, Rempel DL, Frieden C, Gross ML (2015) Continuous and pulsed hydrogen-deuterium exchange and mass spectrometry characterize CsgE oligomerization. *Biochemistry* 54(42):6475–6481.
42. Madej T, et al. (2014) MMDB and VAST+: Tracking structural similarities between macromolecular complexes. *Nucleic Acids Res* 42(Database issue):D297–D303.
43. Bonsor DA, et al. (2009) Allosteric beta-propeller signalling in TolB and its manipulation by translocating colicins. *EMBO J* 28(18):2846–2857.
44. Tian P, et al. (2015) Structure of a functional amyloid protein subunit computed using sequence variation. *J Am Chem Soc* 137(1):22–25.
45. Koo EH, Lansbury PT, Jr, Kelly JW (1999) Amyloid diseases: Abnormal protein aggregation in neurodegeneration. *Proc Natl Acad Sci USA* 96(18):9989–9990.
46. Fowler DM, Koulov AV, Balch WE, Kelly JW (2007) Functional amyloid–from bacteria to humans. *Trends Biochem Sci* 32(5):217–224.
47. Hammer ND, Wang X, McGuffie BA, Chapman MR (2008) Amyloids: Friend or foe? *J Alzheimers Dis* 13(4):407–419.
48. Lee W, Tonelli M, Markley JL (2015) NMRFAM-SPARKY: Enhanced software for biomolecular NMR spectroscopy. *Bioinformatics* 31(8):1325–1327.
49. Güntert P, Buchner L (2015) Combined automated NOE assignment and structure calculation with CYANA. *J Biomol NMR* 62(4):453–471.
50. Buchner L, Güntert P (2015) Systematic evaluation of combined automated NOE assignment and structure calculation with CYANA. *J Biomol NMR* 62(1):81–95.
51. Shen Y, Bax A (2013) Protein backbone and sidechain torsion angles predicted from NMR chemical shifts using artificial neural networks. *J Biomol NMR* 56(3):227–241.
52. Shu Q, Frieden C (2004) Urea-dependent unfolding of murine adenosine deaminase: Sequential destabilization as measured by 19F NMR. *Biochemistry* 43(6):1432–1439.
53. Dunbrack RL, Jr (2002) Rotamer libraries in the 21st century. *Curr Opin Struct Biol* 12(4):431–440.